# Magnetic dichroism in valence-band photoemission spectroscopy of disordered bcc $Fe_xCo_{1-x}$ alloys

S. Ostanin and H. Ebert
*Institute for Physical Chemistry, University of Munich, Theresienstr. 37, D-80333 München, Germany*
(Received 16 June 1998)

A fully relativistic calculation of spin-resolved valence-band photoemission spectra for bcc $Fe_xCo_{1-x}$ alloys is presented that is based on the Korringa-Kohn-Rostoker coherent-potential approximation method of band-structure calculation. The result for the spin-integrated spectra for unpolarized radiation was found to be in very satisfying agreement with corresponding experimental data. For the spin-resolved spectra a pronounced magnetic circular dichroism is predicted that should be observable in a corresponding experiment. [S0163-1829(98)04541-X]

## I. INTRODUCTION

Within the last decade, experiments based on magnetic dichroism and using synchrotron radiation became a powerful tool in the study of the electron structure of magnetic materials.[1,2] The main reason for this is that the dependency of the corresponding spectra on the polarization of the exciting radiation reflects the subtle interplay of spin-orbit coupling and magnetic ordering. For example, a newly developed spin-resolved resonant x-ray photoemission spectroscopy experiment on $2p$ core levels using circularly polarized radiation allows one to measure the local $3d$ spin polarization independent of the orientation of the local moment.[3]

In case of the valence-band photoemission magnetic dichroism in its linear and circular form has been investigated by various experimental groups[4–7] using radiation in the UV regime (VB-UPS). By extending the one-step model of photoemission to the spin-polarized relativistic situation a proper theoretical description of these experiments on transition metal systems could be given by Feder and co-workers.[8]

Valence-band photoemission experiments done with polarized radiation give extremely detailed insight into the electronic structure of the investigated material because of the various selection rules. However, for valence-band photoemission spectroscopy in the x-ray regime (VB-XPS) the $\vec{k}$ selection rule is no longer present.[9,10] A fully relativistic description of VB-XPS for a $Co_xPt_{1-x}$ system allowed us recently[11] to achieve for unpolarized radiation very good agreement between the spin-integrated calculated spectra and available experimental data.[12] In addition it could be shown[11] that a pronounced magnetic dichroism should be observed in a corresponding experiment using circularly polarized radiation—even for angular integrated spectra.

In this contribution a similar study of the valence-band photoemission (VB-PES) for the disordered bcc $Fe_xCo_{1-x}$ alloy system is presented. In particular, the magnetic dichroism has been investigated for various concentrations. In contrast to our previous work on XPS lower photon energies in the UV region have been considered here. As a consequence it was necessary to reconsider the treatment of multiple scattering for the final states. A former attempt to interpret the experimental VB-UPS spectra of the bcc $Fe_xCo_{1-x}$ system was made on a qualitative level using the spin-resolved density of states calculated by the cluster Koringa-Kohn-Rostoker coherent potential approximation (KKR-CPA) method.[13] Quite recently the spin and orbital polarized relativistic version of the KKR-CPA method was proposed and applied to bcc $Fe_xCo_{1-x}$ alloys.[14] This rather sophisticated band structure formalism is used within the present work to study possible magnetic dichroism in the VB-PES of this system.

## II. EXPRESSION FOR THE PHOTOCURRENT

An expression for the intensity $I(E,\vec{k},m_s;\omega,\vec{q},\lambda)$ of the photoelectron current observed in VB-PES can be derived by starting from Fermi's ''golden rule:'' [15]

$$I(E,\vec{k},m_s;\omega,2\vec{q},\lambda) \propto \sum_{\text{initial states } i} \left| \int d^3r \, \phi^{\text{final}\times}_{\vec{k}m_s}(\vec{r},E) X_{\vec{q}\lambda}(\vec{r}) \phi_i(\vec{r},E_i) \right|^2 \times \delta(E-\omega-E_i). \quad (1)$$

Here the operator $X_{\vec{q},\lambda} = -e\vec{\alpha}\cdot\vec{A}_{\vec{q}\lambda}$ describes the interaction of the electrons and the radiation field with the vector potential $\vec{A}_{\vec{q}\lambda}$ representing the radiation with energy $\omega$, wave vector $\vec{q}$, and polarization $\lambda$. To account properly for all relativistic effects, the electron current density operator has been expressed in terms of the vector of Dirac matrices $\vec{\alpha}$.[16]

In Eq. (1) it has been assumed that the detector selectively counts photoelectrons with energy $E$, wave vector $\vec{k}$, and spin polarization $m_s$. The corresponding final state $\phi^{\text{final}}_{\vec{k},m_s}$ is therefore identical to a time-reversed LEED state $\phi^{\text{final}}_{\vec{k}m_s} = T\phi^{\text{LEED}}_{-\vec{k}-m_s}$ ($T=-i\sigma_y K$ is the time reversal operator[17]). Using relativistic multiple scattering theory for spin-polarized systems, the final states may be expressed by[18]

 

$$\phi^{\text{final}}_{\vec{k}m_s}(\vec{r}_n,E') = 4\pi\sqrt{\frac{E'+c^2}{2E'+c^2}}\sum_{\Lambda} i^{-l}C^{-m_s}_{\Lambda}Y^{\mu+m_s}_{l}(-\hat{k}) \times\sum_{m} e^{i\vec{k}\cdot\vec{R}_m}\sum_{\Lambda'}\tau^{nm*}_{\Lambda'\Lambda}(E')[TZ_{\Lambda'}(\vec{r}_n,E')]. \tag{2}$$

Here $E'=E+\omega$, $\tau^{nm}_{\Lambda'\Lambda}$ is the scattering path operator connecting lattice sites at $\vec{R}_m$ and $\vec{R}_n$ while $Z_{\Lambda'}$ is a regular solution to the single site Dirac equation for the potential well centered at site $\vec{R}_n$. The quantities $C^{m_s}_{\Lambda}$ and $Y^{m_l}_{l}$ are the Clebsch-Gordon coefficients and the spherical harmonics according to the conventions of Rose[16] with the relativistic quantum numbers $\Lambda=(\kappa,\mu)$.

The manifold of initial states $\phi_i$ in Eq. (1) together with the delta function may be represented by the imaginary part of the electronic Green's function:[19]

$$G^{+}(\vec{r}_n,\vec{r}'_m,E)=\sum_{\Lambda\Lambda'} Z_{\Lambda}(\vec{r}_n,E)\tau^{nm}_{\Lambda\Lambda'}(E)Z^{\times}_{\Lambda'}(\vec{r}'_m,E) - \sum_{\Lambda} Z_{\Lambda}(\vec{r}_<,E)J^{\times}_{\Lambda}(\vec{r}_>,E)\delta_{nm}, \tag{3}$$

where $J_\Lambda$ is the irregular solution to the single site Dirac equation. Inserting Eqs. (3) and (2) into Eq. (1) allows one to deal with spin- and angular-resolved UPS in a fully relativistic way in complete analogy to the approach of Feder and co-workers.[8] This leads to the following expression for the photocurrent:

$$I(E,\vec{k},m_s;\omega,\vec{q},\lambda)=(4\pi)^2\sqrt{E'}\,\frac{E'+c^2}{2E'+c^2}\,\mathrm{Im}\sum_{\Lambda\Lambda''}(i^{l-l''})C^{-m_s}_{\Lambda}C^{-m_s}_{\Lambda''}Y^{\mu+m_s*}_{l}(-\hat{k})Y^{\mu''+m_s*}_{l''}(-\hat{k})\sum_{m,m'} e^{-i\vec{k}(\vec{R}_m-\vec{R}_{m'})} \times\sum_{n,n'}\sum_{\Lambda',\Lambda'''}\tau^{nm}_{\Lambda'\Lambda}(E')\tau^{n'm'*}_{\Lambda'''\Lambda''}(E')\left[\sum_{\Lambda_1\Lambda_2}\tau^{nn'}_{\Lambda_1\Lambda_2}(E)M^{\vec{q}\lambda}_{\Lambda'\Lambda_1}M^{\vec{q}\lambda*}_{\Lambda'''\Lambda_2}-\sum_{\Lambda_1} I^{\vec{q}\lambda}_{\Lambda'\Lambda_1\Lambda'''}\right]. \tag{4}$$

Here the matrix elements $M^{\vec{q}\lambda}_{\Lambda\Lambda'}$ and $I^{\vec{q}\lambda}_{\Lambda\Lambda'\Lambda''}$ with respect to the operator $X_{\vec{q}\lambda}$ are given by

$$M^{\vec{q}\lambda}_{\Lambda\Lambda'}=\int d^3r[TZ_{\Lambda}(\vec{r},E')]^{\times}X_{\vec{q}\lambda}(\vec{r})Z_{\Lambda'}(\vec{r},E) \tag{5}$$

and

$$I^{\vec{q}\lambda}_{\Lambda\Lambda'\Lambda''}=\int d^3r\int d^3r'[TZ_{\Lambda}(\vec{r},E')]^{\times}X_{\vec{q}\lambda}(\vec{r})Z_{\Lambda'}(\vec{r}_<,E) \times J^{\times}_{\Lambda'}(\vec{r}_>,E)X^{\times}_{\vec{q}\lambda}(\vec{r}')[TZ_{\Lambda''}(\vec{r}'),E')]. \tag{6}$$

One should remark here that the last term in Eq. (4)—i.e., the sum over the matrix elements $I^{\vec{q}\lambda}_{\Lambda\Lambda'\Lambda''}$—stems from the second term in the expression for the Green's function in Eq. (3). Thus, it is the only term that is connected with the irregular solutions $J_\Lambda$ and contributes to the photocurrent only if one works with complex energies.

For the XPS regime a number of simplifications can be applied. First, one can assume that XPS primarily probes bulk properties. This means that it is sufficient to deal with the excitation process for a representative unit cell—say at site $\vec{R}_0$. Second, arguments can be given[9,10] that for the XPS regime $\vec{k}$ conservation does not hold any more. As a consequence the photocurrent $I(E,\vec{k},m_s;\omega,\vec{q},\lambda)$ is determined only by the electronic properties within the cell at site $\vec{R}_0$. The corresponding expression gets quite simple if it is averaged with respect to $\vec{k}$ to simulate a powder sample or an angle-integrated spectrum.

Finally, all multiple scattering events for the final state can be ignored[10] for high energies of the exiting radiation. This single scatterer approximation amounts to restricting the sum over sites $\vec{R}_m$ in Eq. (2) to $\vec{R}_m=\vec{R}_n$ and to replacing $\tau^{nm}_{\Lambda\Lambda'}$ by the single-site $t$ matrix $t^{n}_{\Lambda\Lambda'}$. Accordingly, if one is dealing with a randomly disordered alloy it is straightforward to perform the necessary configuration average.[10] In the case of one atom per unit cell one can find the following expression for the photocurrent:[11]

$$I(E,m_s;\omega,\vec{q},\lambda)\propto\sum_{\alpha} x_\alpha\,\mathrm{Im}\sum_{\substack{\Lambda\Lambda''\\ \mu=\mu''}} C^{-m_s}_{\Lambda}C^{-m_s}_{\Lambda''} \times\left\{\sum_{\Lambda_1\Lambda_2}\tau^{00,\alpha}_{\Lambda_1\Lambda_2}(E)\left[\sum_{\Lambda'} t^{0,\alpha}_{\Lambda'\Lambda}(E')M^{\vec{q}\lambda,\alpha}_{\Lambda'\Lambda_1}\right] \times\left[\sum_{\Lambda'''} t^{0,\alpha}_{\Lambda'''\Lambda''}(E')M^{\vec{q}\lambda,\alpha}_{\Lambda'''\Lambda_2}\right]^{*} - \sum_{\Lambda'\Lambda'''\Lambda_1} t^{0,\alpha}_{\Lambda'\Lambda}(E')I^{\vec{q}\lambda,\alpha}_{\Lambda'\Lambda_1\Lambda'''}t^{0,\alpha*}_{\Lambda'''\Lambda''}(E')\right\}. \tag{7}$$

Here $x_\alpha$ is the concentration of component $\alpha$.[10]

Because use of the single scatterer approximation gets questionable the expression in Eq. (7) seems to be no longer applicable for photon energies in the UV regime. This situation has been dealt with by Durham, who developed a nonrelativistic description of the angular-resolved UPS of disordered alloys.[20] Most important, he argues that the configurational average of the product of three Green's functions occurring in the expression for the photocurrent [see Eqs. (4) and (10) of Durham's paper] can be replaced by the product of three configurationally averaged Green's functions because of the different energies involved. This neglect of the vertex corrections is applied as well in the following. Because the calculations presented below are done for still relatively high photon energies ($>40$ eV) it seems justified

to restrict multiple scattering for the final states. The first step to go beyond the single scatterer approximation that is used here is to replace $t^0_{\Lambda'\Lambda}(E')$ in Eq. (7) by the scattering path operator $\tau^{00}_{\Lambda'\Lambda}(E')$. As a consequence the necessary configurational average can be included in a rather straightforward way. This is done—as for the initial states—within the framework of the CPA.

## III. RESULTS AND DISCUSSION

### A. Spectra for unpolarized radiation

Theoretical VB-UPS spectra of disordered bcc $Fe_xCo_{1-x}$ alloys for unpolarized radiation with $\hbar\omega = 40.8$ eV obtained using the scheme described above are given in Fig. 1. As can be seen, these spectra agree very well with corresponding experimental data reported by Weller and co-workers.[13] To allow a direct comparison between the calculated and experimental spectra, we took a Lorentzian broadening for the theoretical curves with a width increasing quadratically with binding energy. The broadening parameters were chosen in accordance with experimental linewidths observed in angle-resolved UPS of dilute ($x \sim 0$) $Fe_xCo_{1-x}$ alloys.[21] In this experimental investigation the linewidth was found to vary approximately linearly with the distance between the line position and the Fermi energy $E_F$ and that with increasing the Fe content the broadening decreases.

As one notes in Fig. 1, the theoretical VB-UPS spectra for the Fe-rich alloys show a prominent peak at a binding energy of $E_b \sim 0.8$ eV. With decreasing Fe content this peak shows a pronounced and continuous shift away from the Fermi energy $E_F$ leading to a binding energy of $E_b \sim 1.3$ eV for $x \sim 0$. At around 3 eV binding energy one notes a shoulder that rapidly gets less pronounced when the Fe concentration decreases. For $x \sim 0.5$ a second prominent peak appears just below $E_F$ at $E_b \sim 0.33$ eV. With increasing Co content the low binding energy peak moves slightly away from $E_F$ and its magnitude increases compared to the first one. All these findings are in very good agreement with experiment (Fig. 1, bottom). Slight differences between theory and experiment with respect to the relative peak heights within the various spectra can partly be ascribed to the problems when subtracting the background for the experimental spectra. Another source is the relatively crude way to account for relaxation processes by broadening the theoretical spectra (see above).

For the paramagnetic case the expression for the photocurrent in Eq. (4) can be simplified to a concentration weighted sum over the products of the $\kappa$-resolved partial density of states (DOS) $n^\kappa_\alpha(E)$ and a corresponding matrix element that smoothly varies with energy.[22] Thus, the XPS spectra map the DOS curves in a rather direct way. Ignoring the complexities introduced by the spin-orbit coupling, this interpretation should essentially hold also for the spin-polarized case. To supply a corresponding explanation for the spectra in Fig. 1 and their variation with composition we give in Fig. 2 the component and spin-resolved DOS of $Fe_{0.4}Co_{0.6}$. Of course these curves are dominated by their $d$ contributions that give rise to most of the features to be seen. Accordingly the discussion below refers primarily to the $d$ part of the various DOS curves. As one notes the partial DOS curves for Fe and Co are typical for the bcc structure. Furthermore, they are very similar and rather structured; i.e., disorder does not have a dramatic impact on these curves because Fe and Co are quite close to one another in the periodic table. Based on Fig. 2 it is obvious to ascribe the shoulder in the VB-UPS spectra at around 3 eV primarily to the double peak in the majority band. The prominent peak at around 0.8 eV binding energy on the other hand stems from an overlap of a relatively sharp peak in the majority DOS and the counterpart in the minority band to the above-mentioned double peak that gives rise to the shoulder.

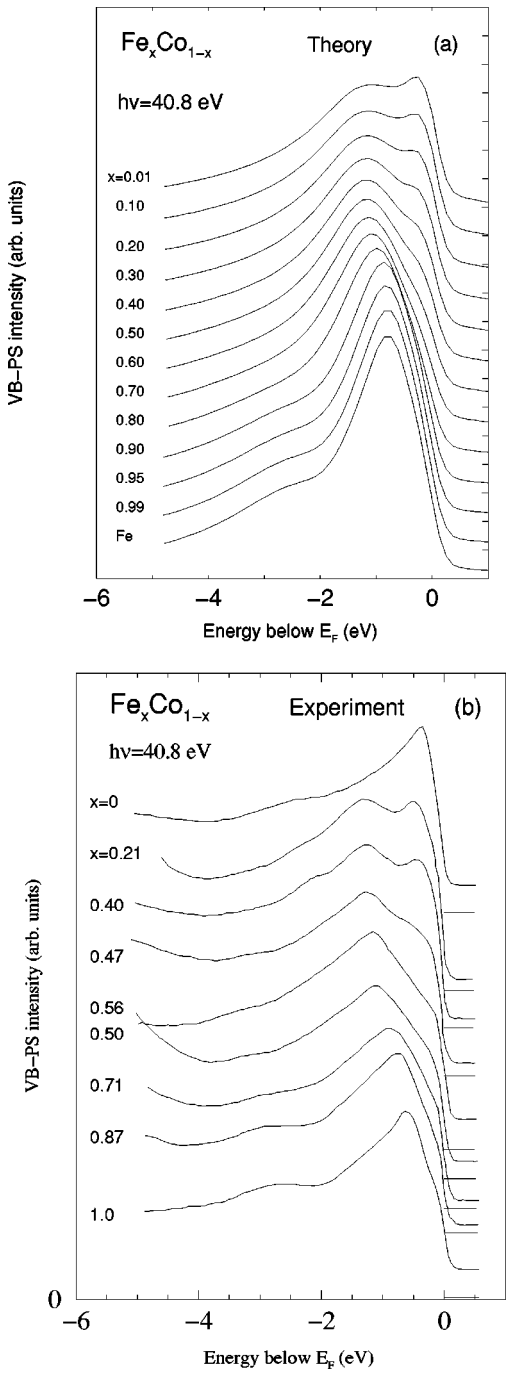


FIG. 1. Theoretical VB-UPS spectra (top) for bcc $Fe_xCo_{1-x}$ for unpolarized radiation and photon energy $\hbar\omega = 40.8$ eV. The corresponding experimental data (bottom) have been taken from Weller *et al.* (Ref. 13). For $x = 0$, i.e., for pure Co, the corresponding sample had hcp structure.

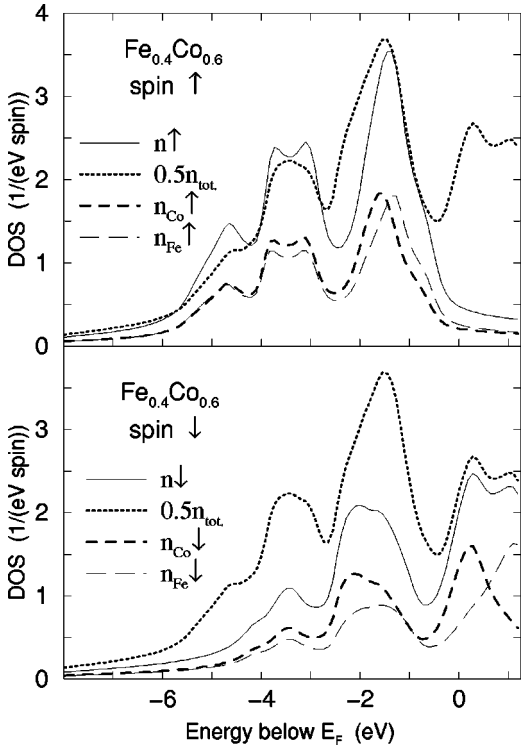


FIG. 2. Component- and spin-resolved density of states curves for bcc $Fe_{0.4}Co_{0.6}$. The upper and lower panels give the results for the majority and minority spin systems, respectively. The component-resolved curves $n_{\alpha}^{m_s}(E)$ ($\alpha$=Fe,Co; $m_s=\uparrow,\downarrow$) are weighted by the corresponding concentration (0.4 and 0.6, respectively). For comparison the total density of states $n(E)$ is given in both panels multiplied by the factor 0.5.

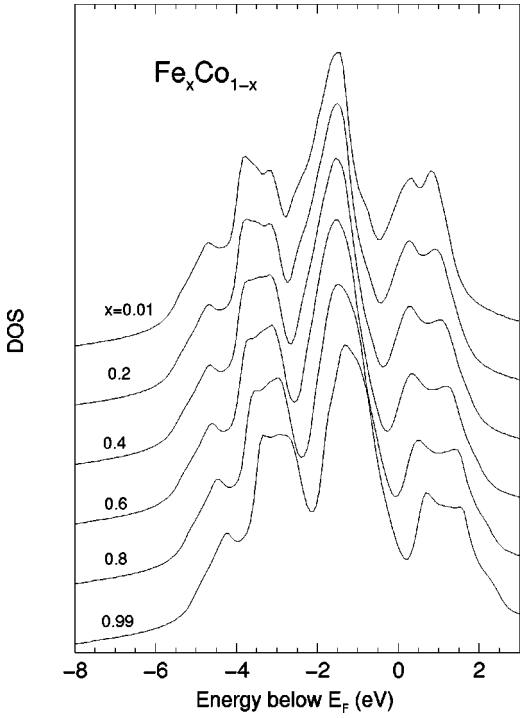


FIG. 3. The total density of states curves for bcc $Fe_xCo_{1-x}$ alloys.

Finally, the peak present at the emission threshold for the Co-rich alloys is ascribed to a peak in the minority DOS that in turn is the counterpart to the majority DOS peak contributing to the main peaks in the spectra. The states giving rise to the peak at the emission threshold are nearly exclusively Co states because of the smaller exchange splitting for Co compared to that of Fe (see Fig. 2). In addition one can also see in Fig. 2 that the Co states are at the average located at higher binding energies as the Fe states because of the higher atomic number. These two main features of the Co and Fe subbands give rise to the variation of the total DOS with variation shown in Fig. 3. Noting that the photoemission cross section for Fe and Co are very similar it is obvious that the VB-UPS spectra in Fig. 1 give a rather direct mapping of the occupied part of these DOS curves. In this favorable case it is even possible to ascribe to the main features of these spectra a certain spin or component character in a rather unambiguous way on the basis of the DOS curves shown in Fig. 2.

### B. Role of multiple scattering for final states

To investigate the role of multiple scattering events for the final states and its influence on the emission spectra the calculation of the theoretical spectra has been redone using Eq. (7). As mentioned this means using the single scatterer approximation appropriate for the XPS regime, while for the calculations of the spectra in Fig. 1 a superior approach has been used replacing the single-site $t$ matrix by the site-diagonal scattering path operator $\tau$. Corresponding results for both approaches are shown in Fig. 4 for $Fe_{0.4}Co_{0.6}$ in a component resolved way. It should be noted that the two sets of spectra have not been renormalized for that comparison. As one can see an improved treatment of multiple scattering for the final states does not introduce any new features in the spectra making sure that even for 40 eV the VB-UPS spectra nearly exclusively reflect the features of the DOS for the initial states. The differences between the two sets of calculation are very similar for the two components and occur primarily at relatively high binding energy. In particular, using $\tau$ instead of $t$ for the final states leads to somewhat broader spectra. All these findings apply for all concentrations, as can be seen in Fig. 5, where the difference between the total spectra obtained for the two approaches are shown. The variation of this difference with energy is very similar for all concentrations. Nevertheless one notes that it is more pronounced for the Co-rich alloys than for the Fe-rich ones.

### C. Circular dichroism

Performing angular-resolved photoemission experiments for disordered alloys seems to be profitable only in some favorable cases for which disorder does not prevent the existence of a rather well-defined dispersion relation.[20]

Another way to get more detailed information than supplied by the plain angular integrated spectra shown in Fig. 1 is to perform a spin analysis of the photoelectrons. Corresponding difference spectra $I_z^{\uparrow}-I_z^{\downarrow}$ are shown in Fig. 6 (bottom) for $z$-polarized radiation. According to the discussion made above these spectra should reflect the spin polarization of the valence band, i.e., the difference in the minority and majority DOS in a rather direct way. In line with this inter-

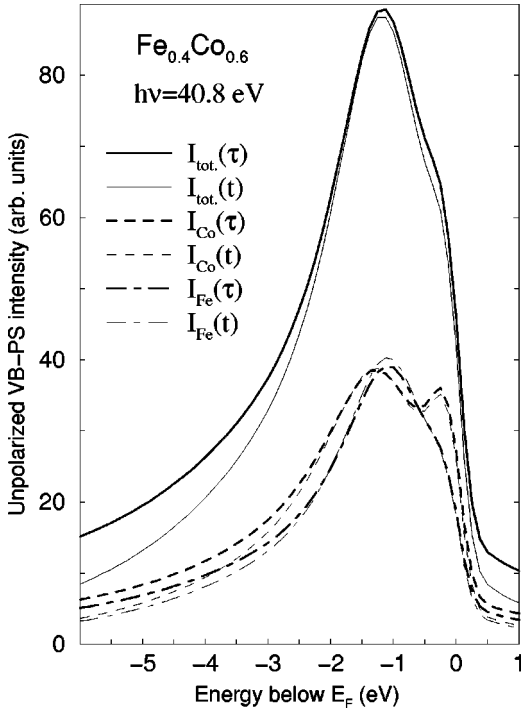


FIG. 4. Theoretical VB-UPS intensity for unpolarized radiation with photon energy $\hbar\omega = 40.8$ eV of $Fe_{0.4}Co_{0.6}$ alloy obtained within the single scatterer approximation (indicated by $t$) and an improved treatment of multiple scattering (indicated by $\tau$) for the final states.

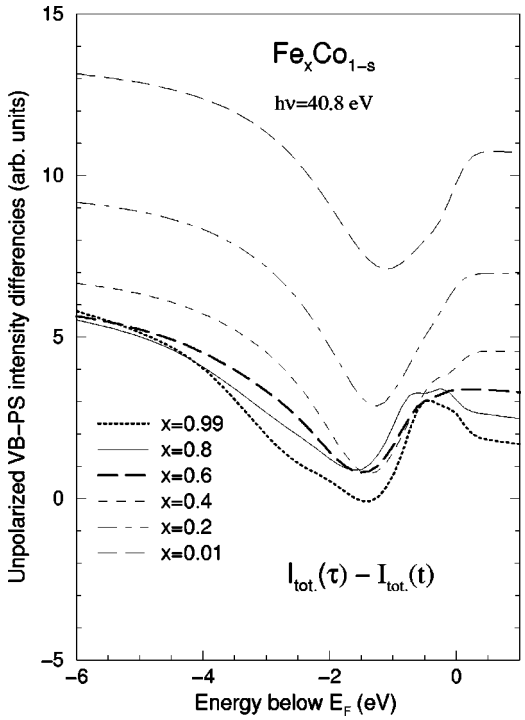


FIG. 5. The differences between theoretical VB-UPS intensities for unpolarized radiation with photon energy $\hbar\omega = 40.8$ eV of $Fe_xCo_{1-x}$ alloy obtained within the single scatterer approximation ($t$) and an improved treatment of multiple scattering ($\tau$) for the final states.

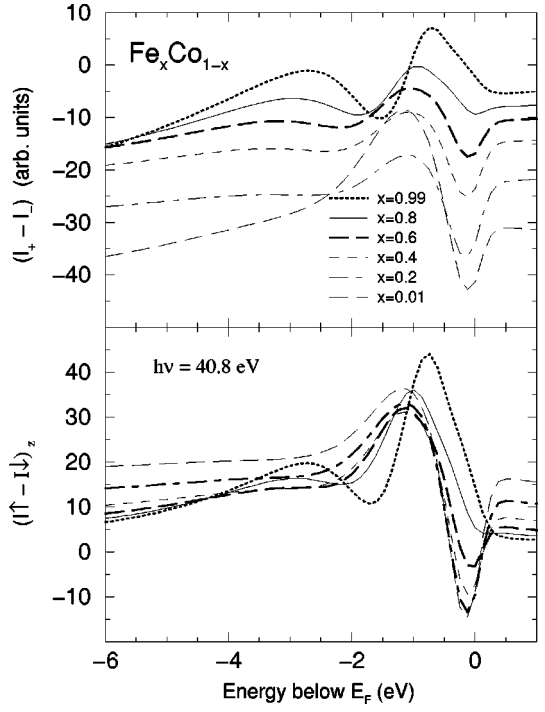


FIG. 6. Theoretical differences in spin-integrated VB-UPS (top) intensity of bcc $Fe_xCo_{1-x}$ at photon energy $\hbar\omega = 40.8$ eV for left (+) and right (−) circularly polarized radiation and also the differences in spin-resolved intensity (bottom) for $z$ polarization of the incident radiation.

pretation and the spin-resolved DOS shown in Fig. 2, the spectra in Fig. 6 (bottom) possess a prominent peak at around 1 eV reflecting a dominating majority DOS. With increasing Co content the minority DOS-related peak at emission threshold evolves and for the Co-rich alloys it has the same amplitude as the main peak.

Another way to probe the magnetic aspects of the electronic structure is to use circularly polarized radiation. The top panel of Fig. 6 shows corresponding dichroic spectra; i.e., the difference $I_- - I_+$ of the photocurrent for left and right circularly polarized light. First of all one notes that this magnetic dichroism is quite pronounced in spite of the angular integrated mode of the spectra. It is much more pronounced than in the case of VB-XPS of $Co_xPt_{1-x}$ investigated recently and should be detectable within a corresponding experiment. For the photon energy assumed here (40.8 eV) the various dichroic spectra are quite similar to the spin-resolved spectra shown in the lower panel of Fig. 6. However, one has to keep in mind that there is no one-to-one relationship between both sets of data. In addition one finds that the spin-orbit induced magnetic dichroism can vary in a very dramatic way with the photon energy as it can be seen from Fig. 7. Here the spectra for a photon energy of 1253.6 eV are compared to those for 40.8 eV. As one notes, the cross section for the XPS regime is strongly reduced and the sign of the dichroism is reversed compared to the UPS spectra.

Finally, combining the spin-resolved mode with the use of circularly polarized radiation dramatically increases the magnetic dichroism. This is demonstrated in Fig. 8 where corresponding results are shown for $Fe_{0.4}Co_{0.6}$. As for the case of

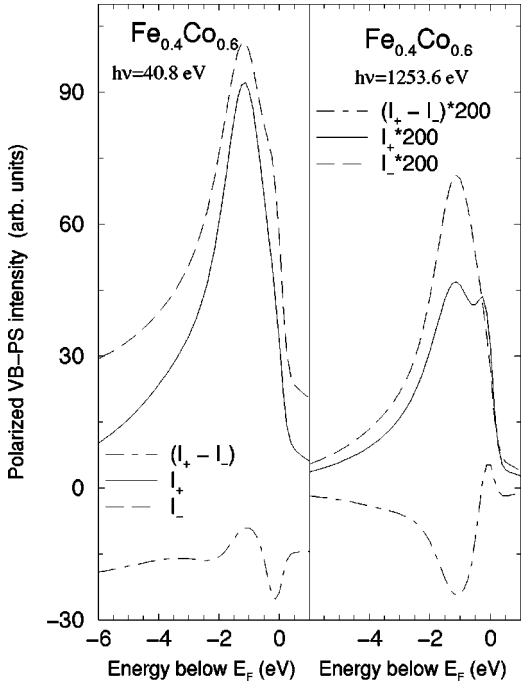


FIG. 7. Theoretical dichroic spin-integrated VB-UPS spectra of $Fe_{0.4}Co_{0.6}$ for circularly polarized radiation with $\hbar\omega = 40.8$ eV (left) and $\hbar\omega = 1253.6$ eV (right) photon energy.

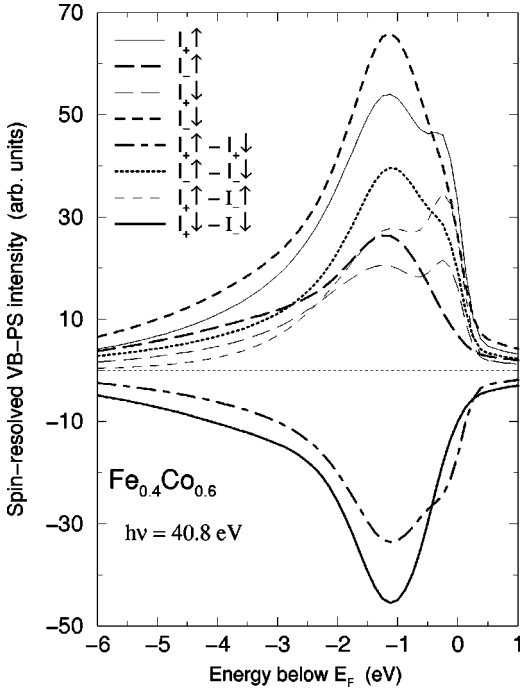


FIG. 8. Theoretical spin-resolved VB-UPS spectra of $Fe_{0.4}Co_{0.6}$ for circularly polarized radiation and photon energy $\hbar\omega = 40.8$ eV.

the angular integrated XPS calculated before no corresponding experimental investigations have been done so far.

## IV. SUMMARY

The scheme developed recently to deal with magnetic dichroism within spin-resolved but angular integrated XPS of dichroic magnetic alloys has been extended to be applicable to the UPS regime. The role of multiple scattering in the final states has been investigated finding that the single scatterer approximation used in the XPS regime is quite acceptable for relatively low photon energies. Applications to bcc-$Fe_xCo_{1-x}$ led to a very satisfying agreement with experiments performed using unpolarized light. Finally, a number of spin-resolved and dichroic spectra have been presented meant to stimulate corresponding experimental work.

## ACKNOWLEDGMENT

This work was supported by the German ministry for education and research (BMBF) under contract 05 621WMA 9 within the program *Zirkular polarisierte Synchrotronstrahlung: Dichroismus, Magnetismus und Spinorientierung.*

[1] *Core Level Spectroscopies for Magnetic Phenomena: Theory and Experiment*, edited by P. S. Bagus, G. Pacchioni, and F. Parmigiani (Plenum, New York, 1995).
[2] *Spin-Orbit Influenced Spectroscopies of Magnetic Solids*, Lecture Notes in Physics Vol. 466 edited by H. Ebert and G. Schütz (Springer-Verlag, Heidelberg, 1996).
[3] B. Sinkovic *et al.*, Phys. Rev. Lett. **79**, 3510 (1997).
[4] C. M. Schneider, P. Schuster, M. S. Hammond, and J. Kirschner, Europhys. Lett. **16**, 689 (1991).
[5] J. Bansmann *et al.*, J. Magn. Magn. Mater. **104**, 1691 (1992).
[6] H. B. Rose, C. Roth, F. U. Hillebrecht, and E. Kisker, Solid State Commun. **91**, 129 (1994).
[7] A. Rampe, D. Hartmann, and G. Güntherodt, in *Spin-orbit Influenced Spectroscopies of Magnetic solids*, Lecture Notes in Physics, Vol. 466, edited by H. Ebert and G. Schütz (Springer, Berlin, 1996), p. 49.
[8] T. Scheunemann, S. V. Halilov, J. Henk, and R. Feder, Solid State Commun. **91**, 487 (1994).
[9] T. Jarlborg and P. O. Nilson, J. Phys. C **12**, 265 (1979).
[10] H. Winter, P. J. Durham, and G. M. Stocks, J. Phys. F **14**, 1047 (1984).
[11] H. Ebert and J. Schwitalla, Phys. Rev. B **55**, 3100 (1997).
[12] D. Weller and W. Reim, Appl. Phys. A: Solids Surf. **49**, 599 (1989).
[13] D. Weller, W. Reim, H. Ebert, D. D. Johnson, and F. J. Pinski, J. Phys. (Paris), Colloq. **49**, C8-41 (1988).
[14] H. Ebert and M. Battocletti, Solid State Commun. **98**, 785 (1996).
[15] P. J. Feibelman and D. E. Eastman, Phys. Rev. B **10**, 4932 (1974).
[16] M. E. Rose, *Relativistic Electron Theory* (Wiley, New York, 1961).
[17] B. Ackermann and R. Feder, Solid State Commun. **54**, 1077 (1985).
[18] H. Ebert and G. Y. Guo, J. Magn. Magn. Mater. **148**, 174 (1995).
[19] P. Strange, H. Ebert, J. B. Staunton, and B. L. Gyorffy, J. Phys.: Condens. Matter **1**, 2959 (1989).
[20] P. J. Durham, J. Phys. F **11**, 2475 (1981).
[21] H. Neddermeyer, L. P. L. M. Rabou, and P. E. Mijnarends, J. Phys. F **14**, 259 (1984).
[22] P. Marksteiner *et al.*, Phys. Rev. B **34**, 6730 (1986).